25th ABCM International Congress of Mechanical Engineering
October 20-25, 2019, Uberlândia, MG, Brazil

COB-2019-0116
NUMERICAL ANALYSIS OF THE LEADING-EDGE BLUNTNESS EFFECT AND ISOLATOR HEIGHT ON A SCRAMJET INLET

João Vitor Siqueira
Aeronautics Institute of Technology. Praça Marechal Eduardo Gomes, 50. Vila das Acácias, 12228-900. São José dos Campos/SP – Brasil
Joaovitormarques22@hotmail.com

Mauricio Antoniazzi Rosa
Institute for Advanced Studies. Trevo Coronel Aviador José Alberto Albano do Amarante 01. Putim, São José dos Campos/ SP - Brasil
mauricioaprosa@gmail.com

Guilherme B. Ribeiro
Aeronautics Institute of Technology. Praça Marechal Eduardo Gomes, 50. Vila das Acácias, 12228-900. São José dos Campos/SP – Brasil
gbribeio@ita.br

Abstract. *Airbreathing hypersonic vehicles can be powered by scramjet (supersonic combustion ramjet) engines, whose inlet requires blunt leading edges in order to overcome the high heat fluxes that are inherent of hypersonic flights. Thus, this work has the purpose of evaluating, through detailed bi-dimensional computational fluid dynamics (CFD) analyses, the influence of the leading-edge bluntness and isolator height on the airflow of a scramjet intake. Results showed that bluntness has the negative effect of increasing the boundary layer separation (BLS) region in the first wedge which is compensated with the positive ones of reducing the high heat flux peak on the reattachment point and the pressure on the second wedge. Both, leading-edge bluntness and isolator height performed great influence on the intake airflow structure. The isolator height, by its turn, had a major effect on the flow separation at the isolator entrance yielding a bubble that increases with the isolator height, although the air mass flow inside the isolator is not much affected. In some circumstances, these shock-wave/boundary-layer interaction (SWBLI) may lead the engine to an unstart condition in which the airflow in the isolator is no proper for scramjet operation.*

Keywords: *Scramjet, hypersonic, CFD, bluntness*

1. INTRODUCTION

The air intake structure of a scramjet engine is in general quite simple and usually does not have moving parts. It uses its own shock-wave structures to slow down and compress the hypersonic airflow to suitable conditions for the fuel combustion in the engine combustor region. Moreover, it is worth mentioning that a great advantage that scramjet engines have over rocket engines is the fact that the scramjet can take more payload per unit take-off mass into orbit which may reduce the mission cost. The oxygen used in the rockets represents more than half of the total rocket mass and therefore, considering the same take-off mass, the vehicle powered by air-breathing engines can carry more payloads (Griffiths, 2005; Smart, 2008; Alcaide, 2007).

Additionally, the inlet must be designed to capture the exact amount of air, at suitable pressure and temperature, to avoid great loss of total pressure and to mitigate drag forces in order to optimize the combustion Smart, 2008; Van Wie, 2000). In the 1940s and early 1950s, hypersonic vehicles aerodynamics followed the supersonic aerodynamics practiced at that time, where the objective was to develop a vehicle with slender body and very sharp leading edge, producing a weak shock wave and consequently a very low wave drag. However, because of the fact that the aerodynamic heating increases with the flight Mach number increase and that the heat transfer to sharp leading edges become extreme in such high Mach numbers, the aerodynamic heating is considered a critical issue which need to be addressed in the development of a feasible hypersonic vehicle. One solution is to use blunt leading edges at the scramjet inlet, since the heating at the stagnation point varies inversely as the square root of the leading-edge radius (Anderson Jr., 1989).

Shock-wave/boundary-layer interactions (SWBLI) can cause flow separation near the corner that may modify considerably the flow field structure. The flow separation increases the temperature and pressure, promoting a peak of wall heat flux at the boundary-layer reattachment point. All these effects may reduce the overall engine performance and

adversely affect the flow properties at the combustor entrance which may even lead to severe conditions of engine unstart (Reynartz et al, 2006). Due to these reasons, the vehicle forebody leading-edge bluntness has an important effect on the flow separation region and the wall heat flux peak. Therefore, once hypersonic flights achieve very high temperatures, a critical part in developing a scramjet engine is to have materials that can withstand such high temperatures. The highest heat fluxes in a scramjet intake take place at the forebody and cowl leading edges.

Considering these aforementioned aspects, this work aims the numerical analysis of the influence of the forebody and cowl leading-edge bluntness, as well as the isolator height, on the intake airflow. All the numerical calculations displayed in this study have been performed using the commercial CFD software ANSYS Fluent, version 15.0.

2. NUMERICAL MODELING

2.1 Governing equations

A mathematical model is necessary for numerically analyzing the blunt leading-edge effects on the hypersonic airflow at scramjet intakes. Therefore, this section presents the governing and constitutive equations for an airflow modeling. The Reynolds-Averaged Navier-Stokes (RANS) equations of continuity (Eq. (1)), momentum conservation (Eq.(2)) and energy (Eq.(3)) are used to numerically calculate the airflow with the ANSYS Fluent. Also to close the system of equations, considering air as a calorically perfect gas, state equations for energy, enthalpy and perfect gas law are considered, such that:

$$\frac{\partial \rho}{\partial t} + \nabla.(\rho\vec{v}) = 0 \tag{1}$$

$$\frac{\partial \rho}{\partial t} + \nabla.(\rho\vec{v}) + \nabla.(\rho\vec{v}\vec{v}) = -\nabla p + \nabla.\left(\bar{\bar{\tau}}_{eff}\right) \tag{2}$$

$$\frac{\partial}{\partial t}(\rho E) + \nabla.[\vec{v}(\rho E + p)] = \nabla.\left[k_{eff}\nabla T + \left(\bar{\bar{\tau}}_{eff}.\vec{v}\right)\right] + S_h \tag{3}$$

$$E = h - \frac{p}{\rho} + \frac{v^2}{2} \tag{4}$$

$$dh = C_p dT \tag{5}$$

$$p = \rho R T \tag{6}$$

where ρ is density, $\vec{v}$ is velocity vector, p is static pressure, E is total energy, k is thermal conductivity, T is temperature, h is enthalpy, C_p is specific heat at constant pressure, R is the gas constant and S_h is the source term that represents energy generation inside the domain, that is zero in the present analysis. The effective stress tensor, $\bar{\bar{\tau}}_{eff}$, is given by Eq.(7).

$$\bar{\bar{\tau}}_{eff} = \mu_{eff}[(\nabla.\vec{v} + \nabla.\vec{v}^T) - \frac{2}{3}\nabla.\vec{v}I \tag{7}$$

where I is the unit tensor and μ is the viscosity. The second term on the right-hand side represents the effect of volume dilation. The subscript in Eq. (3) means the effective values, which adds the turbulent term whenever a turbulent model is in use.

The set of Equations from. (1) to (7) are valid for both inviscid and viscous flows and they can be solved once the initial and boundary conditions are specified. Of course, there will be some modifications in these equations depending on the type of flow such as inviscid or viscous.

An inviscid flow is characterized as a flow that does not consider thermal conductivity, dissipative transport phenomena of viscosity and mass diffusion. Therefore, it is possible to obtain the equations for inviscid flow by dropping the terms involving friction and thermal conduction in Eq. (2) and Eq. (3). The other equations remain the same.

Viscous flows can be modeled as laminar, turbulent or transitional, that is, can be treated either as laminar or turbulent. In the analyses presented in this work, it was used the transition SST model available in Fluent. This model is based on the combination of the SST k-ω transport equations with two other transport equations: intermittency and one for the transition onset criteria, in terms of momentum-thickness Reynolds number (Ansys, 2014).

2.2 Mesh validation

The geometry, freestream airflow and wall temperature were all taken from the work by Neuenhahn and Olivier (2014). In order to guarantee mesh independence in the problem solution, an ordinary mesh analysis has been done. The

mesh refinement analysis considered only the single-wedge cases. The meshes have all been created using the mesh generation ANSYS ICEM software. Two meshes have been created: a regular one and a less refined one. For both meshes, a region along the flat plate up to a distance of 10 mm plus the radius from the wall was considered to be more refined for a more accurate calculation of the physical interactions that exists in the boundary layer. This 10-mm-plus-the-radius distance from the wall ensures that the whole boundary layer, for all cases, is in the more refined region. For the regular mesh, this 10-mm region has 100 nodes that are arranged in a way that the distance from each node grows exponentially from the wall up to the 10-mm-plus-the-radius distance. For the less-refined mesh this 10 mm region has 50 nodes that are arranged in the same way as the regular mesh. Besides the boundary layer, the more refined part of the mesh also better calculates the shock wave on the leading edge. Table 1 shows the number of nodes of the meshes used in this analysis. Analyzing the results obtained from the mesh refinement analyses, it could be stated that there`s very little difference between the results obtained with the regular and the less refined meshes. However, these analyses have been done considering that the selected mesh would be used to calculate cases with different boundary conditions and, in order to guarantee that there would be no mesh-refinement interference in the results, it was decided to use the more refined meshes in the calculations. It is important to highlight that this decision has been made taking into account that there would be little increase of computational cost if the more refined mesh was used.

Table 1. Cell number of the cases of the mesh refinement analyses.

Case	Number of cells
Regular mesh	85134
Less refined mesh	21877

Besides the mesh validation, this work considers the validation of the SST transition model presented by Siqueira J. V. (2016).

3. RESULTS

3.1 Isolator height and leading-edge bluntness effect

In this section it is presented an analysis of the leading-edge bluntness and isolator height effects on the intake airflow. All cases analyzed in this section considered 300 K wall temperature and transition SST viscous model. Figure 1 shows, respectively, the Mach number contours for both leading edges with 0.5 and 1.0 mm of radius and 20 mm of isolator height. It is possible to observe slightly greater boundary layer separations for the 1.0-mm-radius case. The shock-on-lip condition and the bubble at the beginning of the isolator are observed in both cases.

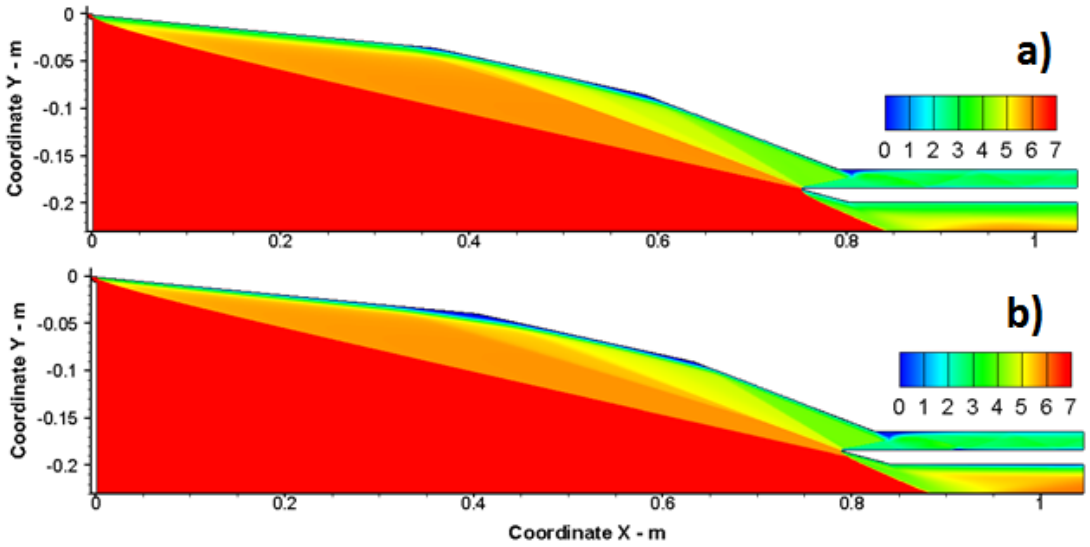

Figure 1. Mach number contours of the inlet with a) 0.5 mm and b) 1.0 mm of leading edge radii, 20 mm of isolator height. 300 K wall temperature and using the SST transitional viscous model.

Figure 2 shows the Mach number contour at the inlet and isolator for two values of isolator heights: 15 mm and 20 mm, both with 0.5 mm of leading-edge radii. It can be clearly seen that the bubble at the beginning of the isolator with 20 mm is quite greater than that for 15 mm isolator height. This is because the reflected shock on the cowl tip of the 20-

mm-height case reaches the upper wall deeper inside the isolator than for the case with 15 mm of isolator height. This bubble partially blocks the airflow into the isolator in a region of low density where the flow recirculation presents quite high temperature. Although the bubble sizes are different in both cases, it seems that the airflow into the isolator, which is limited by the bubble, is basically the same for both isolator heights. Although, it is advised that the reflected shock wave reaches the isolator wall instead of the end of the third ramp in order to reduce the probability of inlet unstarting, this should be done with care because of the high temperature inside of the bubble and the change in the isolator flow yielded by different isolator heights. As can be seen in the Figure 2, the 15 mm reflected shock reaches the isolator wall quite close to the throat, so an isolator height of 20 mm seems to be safer.

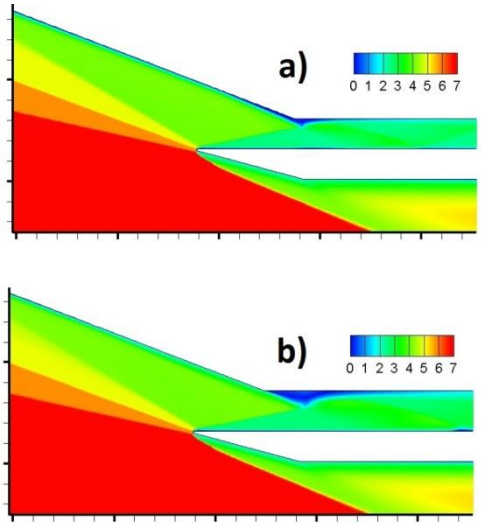

Figure 2. Mach number contour of the isolator of the with a) 20 mm and b) 15 mm of isolator height, 0.5 mm of leading edge radii, 300 K wall temperature and using SST transitional viscous model.

Figures 3, 4 and 5 show, respectively, the contours of the static pressure, static temperature and total pressure for both isolator heights of the cases in Figure 2. As it would be expected, the smaller isolator height produces a shock-wave train with higher frequency inside the isolator which also yields higher average static pressure and temperature inside the isolator, although the highest temperatures are found near the throat for the 20 mm isolator height due to the presence of the bubble there. Regarding the total pressure, which may be used as a measure of the intake efficiency, the contours in 5, show that viscous effects near the walls contribute to reduce even more the total pressure already reduced by the existing shock waves. It can be seen that the greater bubble at the isolator for the 20 mm isolator height, which also influences the downstream boundary layer, has an important role in reducing the total pressure recovery of the intake, consequently reducing its efficiency.

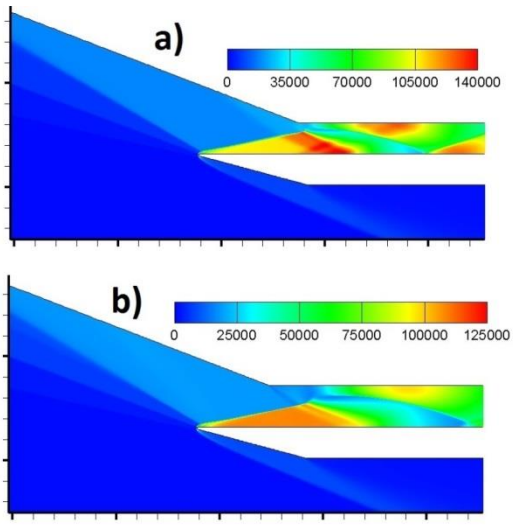

Figure 3. Static pressure of the isolator with a) 15 mm and b) 20 mm.

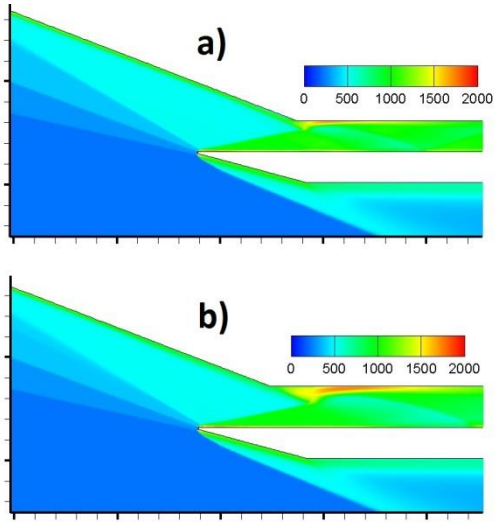

Figure 4 - Static temperature of the isolator with a) 15 mm and b) 20 mm.

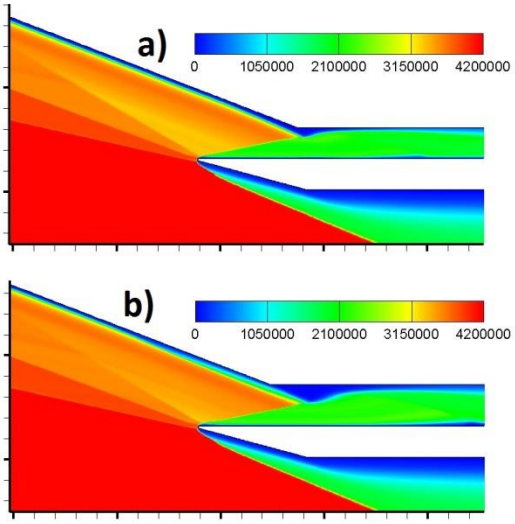

Figure 5 - Total pressure of the isolator with a) 15 mm and 20 mm.

Hypersonic flights achieve very high temperatures, so a critical part in developing a scramjet engine is to have materials that can withstand such high temperatures. The highest heat fluxes in a scramjet intake take place at the forebody and cowl leading edges as previously discussed. Figure 6 and Figure 7 show, respectively, the temperature contours around the 0.5 mm radius forebody and cowl leading edges. It can be observed that the flow temperatures around the leading edges are above 2000 K.

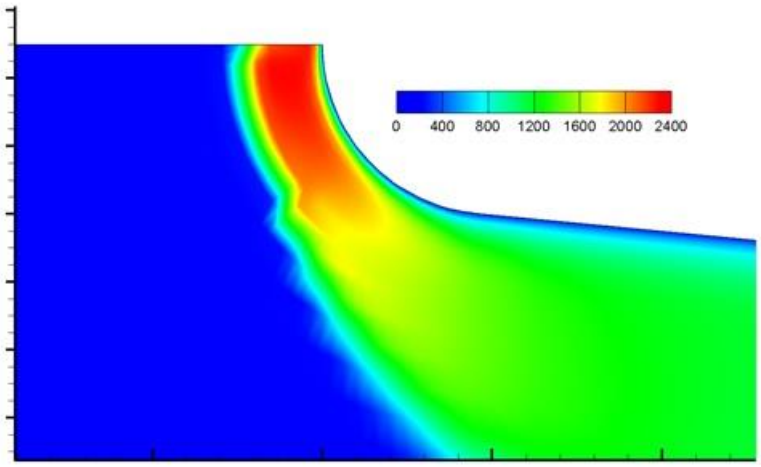

Figure 6. Temperature contour at the forebody leading edge of the inlet.

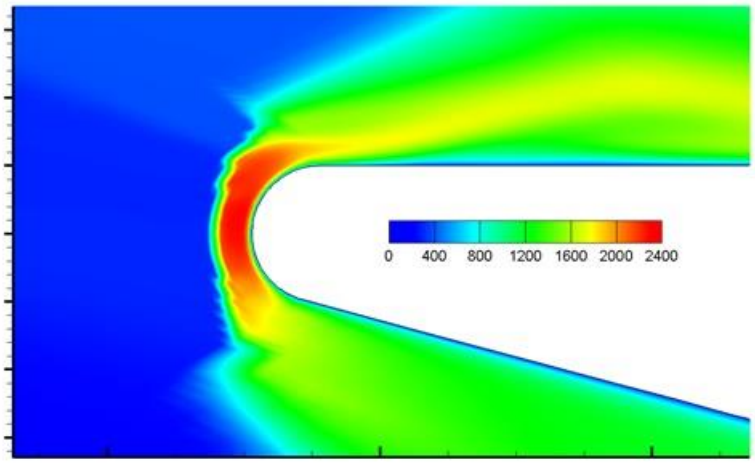

Figure 7. Temperature contour at the cowl leading edge of the inlet.

Figure 8 shows the Stanton number, which is a non-dimensional number that quantifies the heat flux on forebody leading edges with 0.5 and 1.0 mm of radii. It can be seen that the case with 0.5 mm of leading-edge radius presents a heat flux around 25% higher when compared to the case with 1.0 mm of radius.

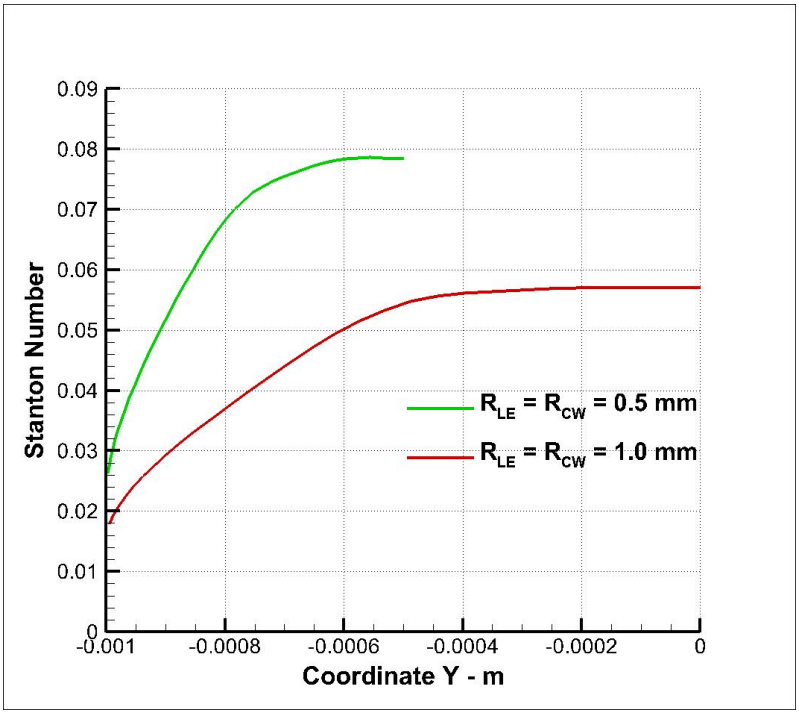

Figure 8 - Heat flux over the forebody leading edge with different radii.

Figure 9 shows the heat flux distribution over the cowl leading edge for the same cases analyzed in Figure 8. Again, the sharper 0.5-mm-radius-leading-edge case presents higher heat flux, although quite smaller than the one on the forebody leading edge. The Stanton number on the cowl leading edge presents different distributions when compared to the forebody ones because of the three ramp shock-wave impingements there.

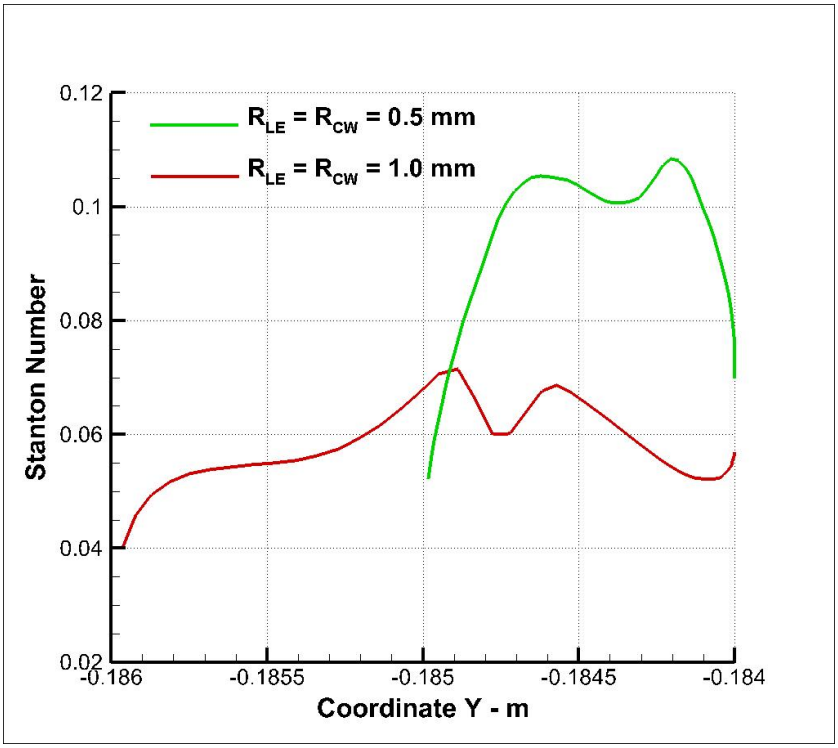

Figure 9 - Heat flux distribution over the cowl leading edge with different radii.

4. SUMMARY AND CONCLUSIONS

Two blunt leading edges have been considered in this analysis at both forebody and cowl: 0.5 mm and 1.0 mm of radii. Two isolator heights have been considered: 15 mm and 20 mm. The greater the isolator height the deeper inside the isolator the reflected shock wave hits its upper wall, which reduces the chance of engine unstart. This generates a big bubble there which makes the airflow to be more expanded inside the isolator. Calculations show evidences that greater isolator heights result in lower static pressure and heat flux distributions on the isolator walls. The temperature is usually higher near the upper wall of the isolator even for higher isolator heights because of the hot bubble at the isolator entrance. Regarding the total pressure, it could be seen that the 20-mm-isolator-height-case features a greater boundary layer separation that consequently decreases the total pressure and therefore the inlet efficiency. Temperature contour analyses show that both forebody and cowl leading edges achieved temperatures above 2000 K behind the bow shock, so it is important to have leading edges with some bluntness in order to reduce the heat flux, even small radii as studied here makes a lot of difference. Leading edge bluntness does not affect much the heat flux distribution on the isolator walls, but it is reduced by approximately 20% by increasing the isolator height from 15 mm to 20 mm.

The present work reached its objective which was, through 2D numerical calculations, to study the effects of leading edge bluntness and isolator height on the airflow of suggested intake geometry.

5. ACKNOWLEDGEMENTS

The authors would like to thank the financial support from FAB (Brazilian Air Force) and CAPES.

6. REFERENCES

ALCAIDE, R. L. M. Investigação da combustão supersônica em túnel de choque hipersônico. 2007. 97f. Dissertação (Mestrado em Engenharia Aeronáutica e Mecânica) – Instituto Tecnológico de Aeronáutica, São José dos Campos.

ANDERSON JR., J.D. Hypersonic and high temperature gas dynamics. New York: McGraw-Hill Book, 1989. 690 p. (McGraw-Hill series in aeronautical and aerospace engineering).

ANSYS, ANSYS fluent 15.0 user's guide, Canonsburg, 2014.McConnell, K.G. and Varoto, P.S., 2008. *Vibration Testing: Theory and Practice*. John Wiley & Sons, New Jersey, 2nd edition.

GRIFFITHS, A. D. Development and demonstration of a diode laser sensor for a scramjet combustor. 2005. 149 f. Thesis (Doctor of Philosophy) – The Australian National University, Australia.

NEUENHAHN, T.; OLIVER, H. Influence of the wall and temperature and the entropy layer effects on double wedge shock / boundary Layer interactions. In: AIAA/AHI SPACE PLANES AND HYPERSONIC SYSTEMS AND TECHNOLOGIES CONFERENCE, 14., 2014, Canberra. Proceedings… Reston: AIAA, 2006. p. 1-11.

REINARTZ, B.; BALLMANN, J.; BOYCE, R. Numerical investigation of wall temperature and entropy layer effects on double wedge shock / boundary layer interactions. Inj: AIAA/AHI SPACE PLANES AND HYPERSONIC SYSTEMS AND TECHNOLOGIES CONFERENCE, 14., 2006, Canberra. Proceedings… Washington, DC: AIAA, p. 1–11, 2006.

SIQUEIRA, J. V. A computational study of the leading-edge bluntness and isolator height effects on the 14-X scramjet intakes. 2016. 138p. Thesis (M. Sc. in Space and Technology) - Instituto Tecnológico de Aeronáutica. São José dos Campos.

SMART, M. Scramjets. In: ADVANCES on propulsion technology for high-speed aircraft. Neuilly-sur-Seine, France: RTO, 2008, p. 1–38. (RTO-EN-AVT-150-09)

VAN WIE, D.M., Scramjet Inlets. In: CURRAN, E. T., MURTHY, S. N. B. (Ed.), Progress in astronautics and aeronautics: scramjet propulsion, v. 189, Reston: American Institute of Aeronautics and Astronautics, 2000 chap 7, p. 447-511.

7. RESPONSIBILITY NOTICE

The authors are the only responsible for the printed material included in this paper.